Progress In Electromagnetics Research C, Vol. 86, 233–245, 2018

Evaluation of a New Dual-Rotor Hybrid Excitation Brushless Motor

Libing Jing*, Jia Cheng, Qixing Gao, Ting Zhang, and Ying Lin

Abstract—This paper presents a novel topology of a dual-rotor hybrid excitation motor (DRHEM), which combines outer permanent magnet synchronous motor (PMSM) and inner doubly salient electromagnetic motor (DSEM). The structure and combination criterion of the DRHEM are introduced and studied. A new type of intermediate stator structure has been adopted and fixed in the form of stator fasteners. The electromagnetic field of the motor is analyzed, and optimization methods are proposed for reducing the cogging torque and superimposing the back electromotive force. Furthermore, to verify the theoretical analysis, experimental tests are conducted, and the torque-speed and output power-speed characteristics are compared under various speeds conditions. The results verify the electromagnetic design well.

1. INTRODUCTION

Hybrid excitation motors (HEM), which have two coexisting excitation sources: permanent magnet (PM) excitation and electromagnetic excitation, aim at combining advantages of permanent-magnet excitation motors and electromagnetic excitation motors [1–3]. With excitation current variable introduced, PM machines can get enhanced in performance of magnetic regulation so make them no longer only rely on the armature winding DC component to adjust the electromagnetic field [4–7].

Some comparisons and analyses for HEM were described in [8, 9], where HEM can be divided into the following two groups: series hybrid excitation machines (SHEM) and parallel hybrid excitation machines (PHEM). The SHEM has simple structures and better regulation of flux density. However, the flux generated by the excitation winding passes directly through the permanent magnet, which may produce demagnetization problem. The PHEM can realize physical separation among the excitation windings and PMs, which can avoid demagnetization of PMs. Besides, relatively small reluctance in the electromagnetic excitation portion (without PM) will improve the excitation current utilization ratio and reduce excitation loss. However, due to complexity of the machines, the PHEM of different structures still has its own problems [10–12]. The HEM needs to develop in the direction of simple structure, compact magnetic circuit structure, high power density, good performance of magnetic regulation and high reliability [13, 14]. A novel direct-driving motor successfully embeds a permanent magnet brushless motor (PMBM) into a concentric magnetic gear (CMG). The PMBM and CMG share a common high-speed rotor [15]. A new kind of PM machines have both stator and rotor PM excitations, namely, dual-PM excited machines. The key is to rely on the PM-iron structure in the machine to provide both PM excitation and flux modulation. Besides the fundamental field component in the air-gap, some other predominant harmonics introduced by the flux modulating effect can also contribute to the electromagnetic torque production. This kind of machines can be designed with high torque density [16]. The doubly complementary stator-PM machines employ two complementarities in the structure, as one exists in double rotors, and the other exists in the units belonging to same phases. This machine could

Received 1 June 2018, Accepted 23 August 2018, Scheduled 6 September 2018

* Corresponding author: Libing Jing (jinglibing163@163.com).

The authors are with the College of Electrical Engineering & New Energy, China Three Gorges University, Yichang 443002, China.

obtain good sinusoidal back-EMF waveform, small torque ripple, and high PM utilization factor due to the doubly complementary characteristic [17].

This paper presents a novel topology of the DRHEM which can combine advantages of dual-rotor machine structure and PHEM performance. Outer PMSM can ensure the efficient operation of motor, and inner DSEM can widen flux regulation range. At the same time it can give a brushless structure for the motor. DRHEM inherits the structure advantages of dual-rotor machine which can be seen from that the two portions (PMSM and DSEM) share one middle stator and a set of armature windings. In addition, the structure and combination criterion are introduced; the optimization method for reducing cogging torque of PMSM and improving phase EMF waveform of DSEM is given for the DRHEM. The research results demonstrate that the proposed DRHEM can achieve better field-regulating, more efficient operation and lower loss than traditional PHEM. The excellent operation characteristics of the DRHEM make it an important application in the field of aviation power supply starting system and electric vehicle.

2. STRUCTURE AND DESIGN CRITERIA

2.1. Structure and Principle

Basic structure of the proposed DRHEM is shown in Fig. 1. The inner rotor and outer rotor respectively constitute the DSEM portion and PMSM portion with the same middle stator. The inner rotor and outer rotor are attached to a rotating shaft by the steel plate and rotate in the same direction at the same speed. Meanwhile, the teeth and slots are opened at the inner and outer sides of the stator simultaneously so that the armature winding wire can pass the middle stator from inner slots to outer slots. Therefore, the total back electromotive force (EMF) of the armature winding of HEM is the sum of DSEM portion and PMSM portion.

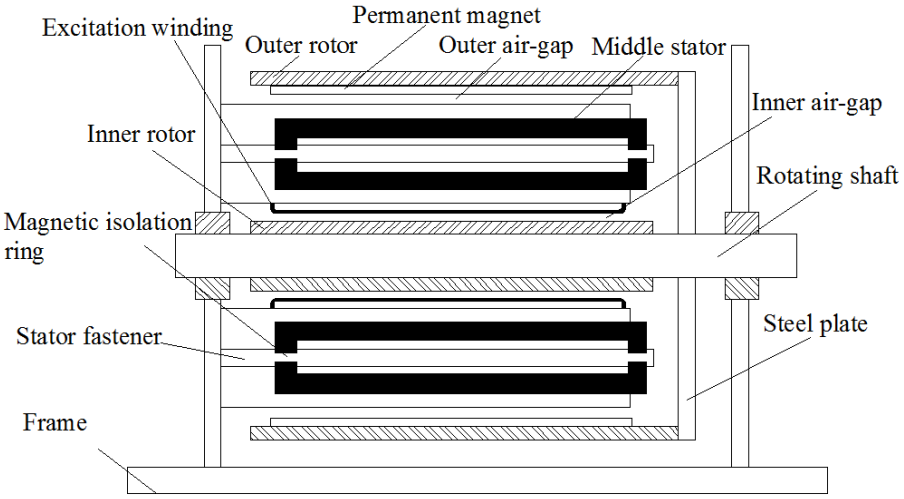

Figure 1. Structure of the proposed DRHEM.

For the DRHEM, permanent-magnet excitation portion and electric excitation portion have radially parallel distribution. On the magnetic circuit, the two portions are independent of each other; however, on the electric circuit, the two portions are coupled with each other because they share a set of armature windings. The isolation on the magnetic circuit does not affect the mutual superposition of the back-EMF of PMSM and DSEM, so as to achieve the characteristics of the magnetic field regulation.

As shown in Fig. 2, permanent magnetic excitation flux remains constant in no-load; however, the magnitude and direction of electrical excitation flux can be adjusted by the exciting current. The flux φ across the armature winding of DRHEM can be expressed as:

$$\varphi = \varphi_{pm} + \varphi_{em} \tag{1}$$

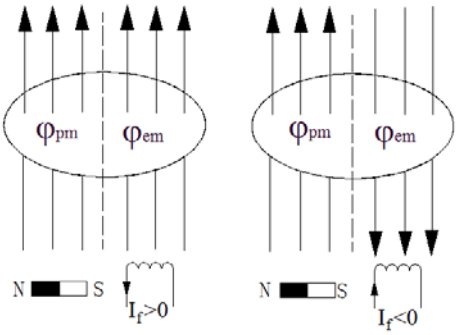

Figure 2. Flux control principle of hybrid excitation.

2.2. Design Criteria

The electric frequency of DSEM and PMSM can be respectively expressed as:

$$f_e = n \cdot p_e/60 \tag{2}$$

$$f_s = n \cdot p_s/60 \tag{3}$$

where p_e is the number of DSEM rotor poles; p_s is the number of PMSM pole pairs.

The DRHEM needs to realize the combination of the PMSM portion and DSEM portion, and the basic principle of combination is to ensure that the armature windings of the two portions can be directly in series. As can be seen from Eqs. (2) and (3), it is the basic combination criteria that pole pair number of PMSM must be the same as pole number of DSEM to ensure the equal electrical frequency of the two portions.

In this paper, a 12/8-pole DSEM is taken as an example to be an electric excitation portion of DRHEM. According to the above matching principle, PMSM should be 16 poles. In addition, the cog number and winding form of PMSM is also a key component to achieve motor energy conversion. In order to facilitate winding connection, the teeth number of PMSM is generally an integer multiple of the stator pole number of DSEM. So, the case where the teeth number of PMSM is 12, 24, 36 will be discussed in the follows. The most suitable number of teeth and winding form will be determined by calculation of winding coefficient and analysis of magnetic motive force (MMF) below.

The winding coefficient is one of the important indexes to evaluate the matching of the pole/slot number of PMSM. The evaluation standard of the winding coefficient is to take the fundamental harmonic wingding coefficient as the maximum and the harmonic coefficient as low as possible. Winding coefficient k_{wv} of V_{th} harmonic can be derived as:

$$k_{wv} = k_{pv} \cdot k_{dv} \tag{4}$$

where k_{pv} is the short-pitch coefficient of Vth harmonic, and k_{dv} is the harmonic distribution coefficient of Vth harmonic.

The specific method and application scope of the winding coefficient calculation for single-layer and double-layer winding are shown in [18]. Table 1 shows the calculation results of the fundamental winding coefficient of the above 6 cases.

For 12-slot/16-pole and 24-pole/16-pole motors, the fundamental winding coefficients of both single-layer and double-layer winding are 0.866. On the other hand, for 36-solt/16-pole motors, the fundamental winding coefficients of both single-layer and double-layer windings are 0.617, far less than 0.866. Therefore, this paper will not consider the combination of 36-slot/16-pole.

Harmonic analysis of the MMF is another important aspect to investigate whether pole-slot combination and winding form is reasonable. Though some of the pole-slot combinations have high fundamental harmonic coefficient, MMF of them may contain severe harmonics which will lead to low-level force wave vibration or result in unbalanced magnetic pull.

For 24-slot/16-pole permanent magnet motors, relative amplitude distribution of the harmonic MMF is shown in Fig. 3. When a single-layer winding is used, subharmonic MMF larger than the

Table 1. Calculation result of the fundamental winding coefficient.

Number of plot/slot \ Winding form	Singlelayer	double-layer
12-slot/16-pole	0.866	0.866
24-slot/16-pole	0.866	0.866
36-slot/16-pole	0.617	0.617

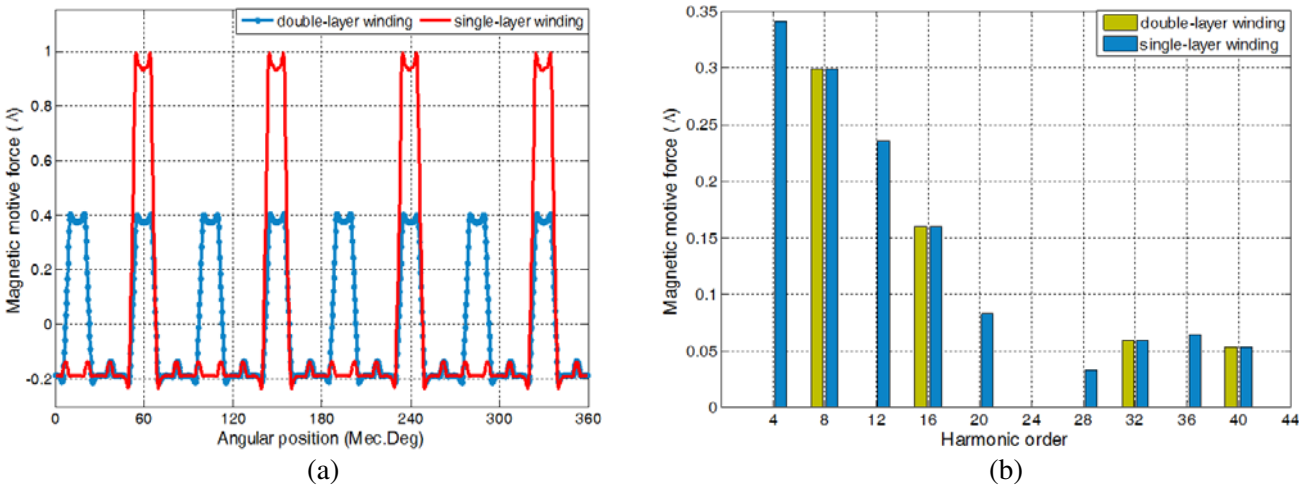

Figure 3. MMF for 24-slot/16-pole permanent magnet motor. (a) MMF waveform. (b) MMF harmonic.

fundamental harmonic will appear, which can produce p/2 order force wave. Therefore, 24-slot/16-pole permanent magnet motor is suitable for using a double-layer winding structure and should be avoided for single-layer winding.

For 12-slot/16-pole permanent magnet motors, relative amplitude distribution of the harmonic MMF is shown in Fig. 4. Both single-layer and double-layer windings can produce subharmonic MMF whose pole-pair number is p/2, and amplitude is 1.9 times of the fundamental harmonic amplitude, which will produce p/2 order force wave. Meanwhile, single-layer winding can produce extra subharmonic MMF whose pole-pair number is p/4, and amplitude is 2.1 times of the fundamental wave amplitude, which will produce p/4 order force wave at the same time. So, 12-slot/16-pole combination should also be avoided to use. In summary, when DSEM portion is 12/8-pole, 24-slot/16-pole double-layer winding form in PMSM portion is the most matching with that.

In order to achieve an efficient combination of the two portions, a special stator structure is adopted as the common stator of PMSM and PSEM. The structure and section of middle stator are shown in Fig. 5(a) and Fig. 5(c), respectively. The intermediate stator can not only realize the combination of the two portions of the motor, but also improve the power density of the motor and offset the magnetic pull of the internal and external portions [19].

The inner stator pole and outer stator slot of middle stator constitute a double air-gap structure with inner rotor and outer rotor, which increases the effective air-gap area of the motor and the winding coil number of the motor, even produces a larger induction electromotive force at a lower speed. The DSEM portion and PMSM portion share a set of armature windings. The armature windings pass through the stator slot of PMSM to the stator pole of DSEM and achieve direct series in the intermediate stator. The back-to-back winding form makes the end length of the winding not increase with the increase of the diameter of the motor. Meanwhile, the back-to-back winding end is so short that it can

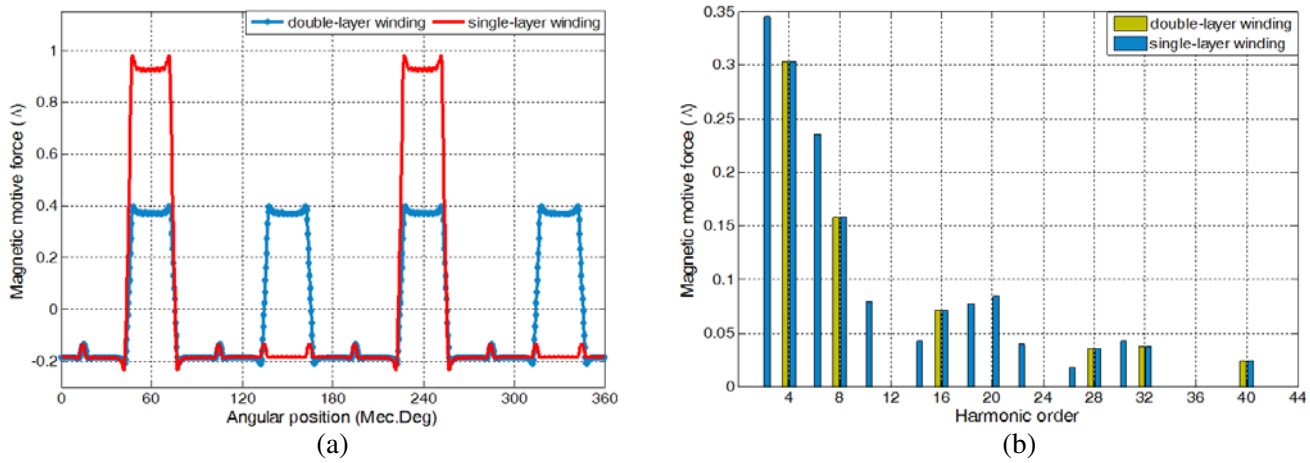

Figure 4. MMF for 12-slot/16-pole permanent magnet motor. (a) MMF waveform. (b) MMF harmonic.

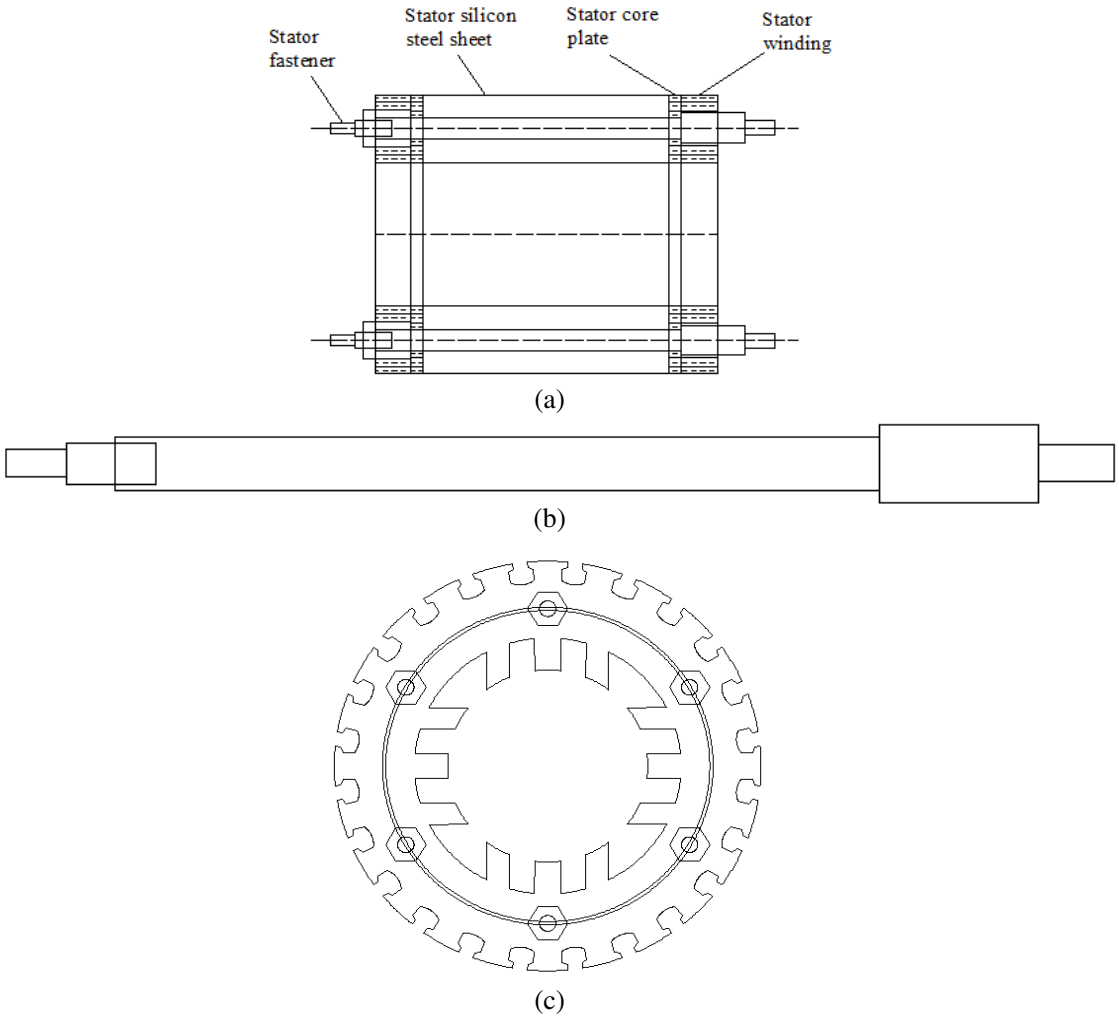

Figure 5. Assembly diagram of stator. (a) Structure of middle stator. (b) Section of stator fastener. (c) Section of Middle stator.

reduce winding resistance and useless loss [20].

There is a magnetic isolation ring in the middle stator to keep two portions of the motor independent of each other in the magnetic circuit. Because of the special structure of the motor, a stator fastener, which can be concentric with the inner rotor, middle stator and outer rotor, is required to fix the stator, and the section of the stator fastener is shown in Fig. 5(b). The ordinary motor has only one air-gap, so the stator can be fixed by the buckle. However, both the inner and outer sides of the DRHEM stator have teeth and slot so that the stator cannot be positioned by the buckle. Therefore, the stator fastener structure is selected to solve the problems mentioned above. The assembly drawings of the stator are shown in Fig. 5. A detailed study of stator fasteners is provided in [21]. The results show that the size, shape and location of stator fasteners are important for stator strength and concentricity. Meanwhile, a suitable stator fastener has little effect on the air-gap flux density, tooth flux density and back-EMF waveform. Therefore, this paper does not take into account the impact of fasteners.

3. OPTIMIZATION AND ADJUSTMENT

In order to optimize the proposed model, the analytical results have been compared with 2-D finite element simulations obtained using ANSYS Maxwell software. In the finite-element analysis, the surfaces of inner and outer rotors yokes as well as those of the ferromagnetic pole-pieces have been modeled by homogeneous Neumann boundary conditions. The mesh in the air-gap and in the slot regions has been refined until convergent results are obtained.

3.1. Cogging Torque Optimization in PMSM Portion

In permanent magnet motors, cogging torque is formed due to the interaction of the permanent magnets and the slot which can generate vibration and noise. In DRHEM, the radius of the PMSM portion is larger than that of the common permanent magnet motors, which will increase the cogging of the proposed motor. Various methods of reducing cogging torque have been given in the literatures, but for outer rotor permanent magnet motors with a large notch and multiple pair pole number, most of the methods are not applicable, or the design is relatively complex. In order to achieve lower cogging torque while not affecting other motor performance, this section gives a simple and effective magnetic pole shift method, which makes the entire outer rotor magnetic pole divided into two parts and lets the two parts respectively shift a certain angle, as shown in Fig. 6.

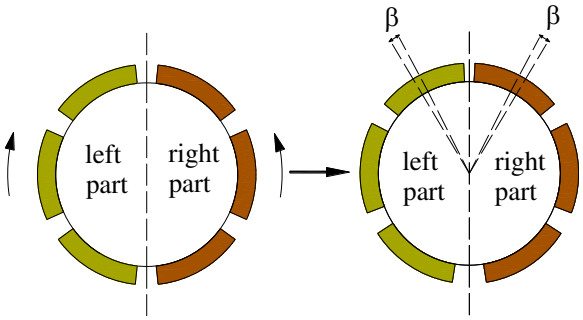

Figure 6. Magnetic pole shift schematic diagram.

Regardless of the electromagnetic saturation, total cogging torque of the magnetic pole uniform for motor can be expressed as:

$$T_{cog} = \sum_{n=1,2,3\ldots}^{\infty} T_{ni} \sin(nN_c\alpha) \tag{5}$$

where T_{ni} is the amplitude of the cogging torque nth harmonics, N_c the least common multiple of the slot number Q_s and poles number $2p$, and α the mechanical angle between the stator and the rotor.

Now rotor magnetic pole is divided into left half part and right half part evenly. The left part of magnetic pole as a whole clockwise rotates β angle, and the right part of the magnetic pole as a whole counterclockwise rotates β angle. The synthetic cogging torque can be expressed respectively as:

$$T_{cog1} = \sum_{n=1,2,3\ldots}^{\infty} T_{ni}[\sin nN_c(\alpha - \beta)] \tag{6}$$

$$T_{cog2} = \sum_{n=1,2,3\ldots}^{\infty} T_{ni}[\sin nN_c(\alpha + \beta)] \tag{7}$$

From Equations (6) and (7) it can be seen that by using this magnetic pole shift method, the final cogging torques T_{cog1} and T_{cog2} can be moved a specific angle with the same phase. Thus, in a rotor by combining these two magnetic poles (clockwise rotation and counterclockwise rotation), the resulting cogging torque components are compensated for each other even the cogging torque can be completely eliminated by an optimum transfer angle. Equation (7) shows the synthetic expression of the cogging torque produced when two parts of the magnetic poles are combined:

$$\begin{aligned} T_{cog} &= \frac{1}{2} \sum_{n=1,2,3\ldots}^{\infty} T_{ni}\{\sin[nN_c(\theta - \beta)] + \sin[nN_c(\theta + \beta)]\} \\ &= \sum_{n=1,2,3\ldots}^{\infty} T_{ni} \sin(nN_c\theta) \cdot \cos(nN_c\beta) \end{aligned} \tag{8}$$

According to Eq. (8), in order to let the cogging torque generated by T_{ni} harmonic is 0, then

$$\cos(nN_c \cdot \beta) = 0 \Rightarrow \beta = \frac{\pi}{2nN_c} \tag{9}$$

According to Eq. (9), for 24-slot/16-pole permanent magnet motors, when n is 1, the optimum value of shift angle β is 1.875° (mechanical angle). A comparison of the cogging torques before and after the magnetic pole shift is given in Fig. 7. The cogging torque of PMSM decreases from 5.2 N to 1.1 N by optimization. Fig. 8 shows the influence of the magnetic pole shift on other performance. P_h A′, B′, C′ is a three-phase induction EMF after the pole shift. As can be seen, the amplitude of the radial air-gap magnetic flux density is not changed, and there is a slight change in the waveform shape. There is no change in waveform of EMF, and there is a little drop in amplitude of EMF. However, these little changes can be ignored completely. So, the compared results show that through the optimization and adjustment of the magnetic pole shift, the motor can greatly reduce the cogging torque amplitude without affecting the other performance.

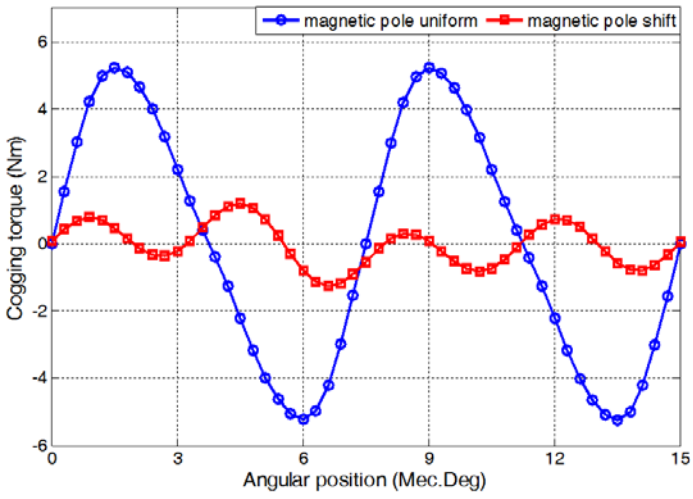

Figure 7. Comparison figure of cogging torques.

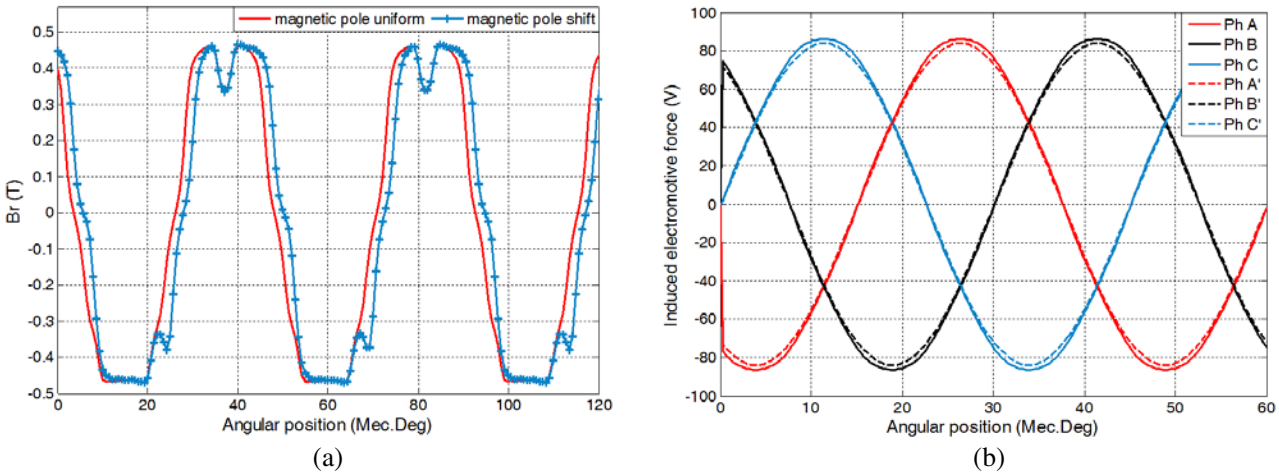

Figure 8. Influence of the the magnetic pole shift. (a) Air-gap flux density waveform. (b) EMF waveform.

3.2. Phase-EMF Waveform Optimization

Each phase armature winding passes through middle stator from DSEM stator pole to PMSM stator teeth. The EMF of each phase is the sum of DSEM portion and PMSM portion. However, the phase EMF waveform of traditional PMSM is different from that of DSEM. So in order to ensure the phase EMF waveform superimposed efficiently, the two portion phase EMF waveform optimization scheme needs to be studied in depth.

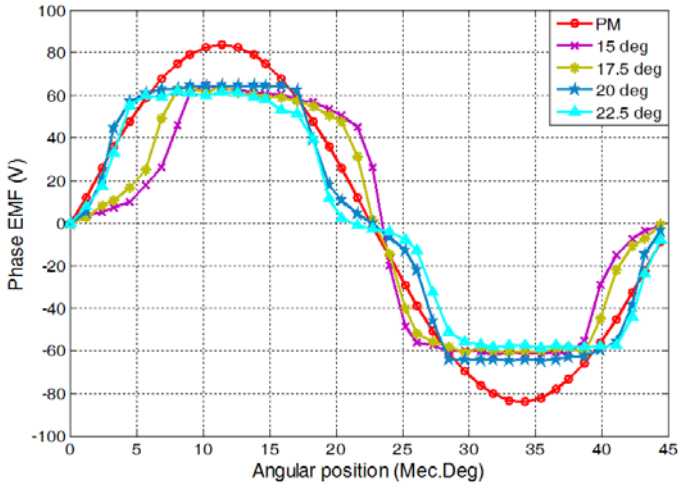

Figure 9. EMF of different rotor pole arcs in DSEM and PMSM.

The phase EMF waveform of the traditional PMSM is a sine wave or trapezoidal wave. When the rotor pole arc is equal to the stator pole arc, the DSEM output power is larger. However, at this time the phase EMF waveforms of the first half period and the second half period are asymmetric to each other, which is significantly different from the phase EMF waveform of PMSM. As shown in Fig. 9, in this paper the phase EMF of the PMSM portion is sinusoidal. For the DSEM portion, with the increase of pole arc, the rotor position angular corresponding to the phase EMF waveform peak value is shifted. When the pole arc is 20 degrees, the waveform shape is near trapezoidal wave, and at this time, the waveform of DSEM portion is close to that of PMSM most. So, the superposition of two parts of phase EMF will be more efficient and reasonable by the improvement and optimization.

4. VERIFICATION OF FEA SIMULATION

By the structure design and model optimization, the configuration of the proposed DRHEM has been basically determined. The key parameters and cross-sectional view of the machine are respectively shown in Table 2 and Fig. 10.

Table 2. Prototype machine specification.

Parameter	Value	
	DSEM	PMSM
Rotor pole number	8	16
Stator slot number	12	24
Stator radius/mm	75	160
Rotor outer radius/mm	74	210
Rotor inner radius/mm	35	166
Air gap length/mm	1	6
Stack length/mm	65	65

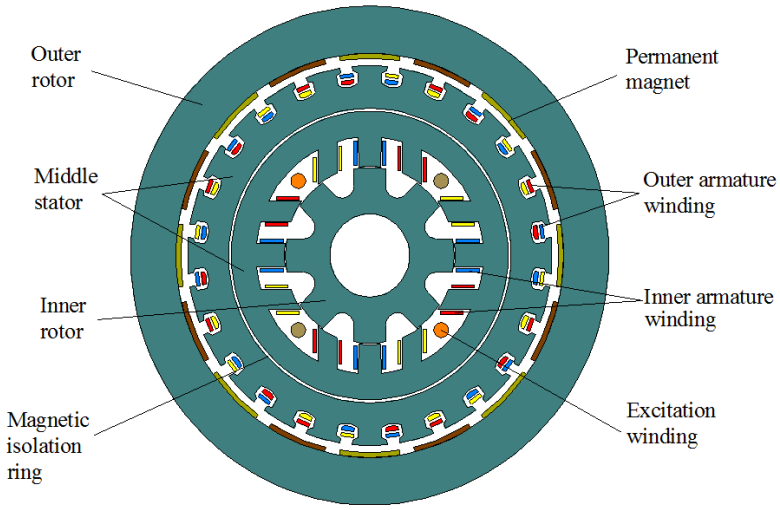

Figure 10. Cross-sectional view of DRHEM.

Figure 11 shows the machine magnetic field lines distribution with different excitation currents. The DSEM portion and PMSM portion are independent of each other on the magnetic circuit due to the existence of magnetic isolation ring. With the increase of the excitation current, magnetic field lines density in DSEM portion increased and field lines density in PMSM portion keep constant.

Figure 12 shows the superposed result of the phase EMF waveforms of two portions. When $I_f > 0$, the phase EMF is increased compared with the case where no excitation current is applied. In contrast, when $I_f < 0$, the phase EMF is weakened. The amplitude of the composite phase EMF can be easily increased or weakened by the control of the excitation current.

Figure 13 shows flux linkage superposition waveforms with different excitation currents, at 1000 rpm. It can be seen that the flux linkage cannot be weakened to 0 completely but keep constant by applying an adequate excitation current, which is decided by unipolar pulse principle of flux linkage in DSEM portion.

Field-circuit coupled model of DRHEM is shown in Fig. 14. Three-phase armature windings are connected to a full-bridge rectifier, and the output is DC terminal voltage. Fig. 15 shows the no-load

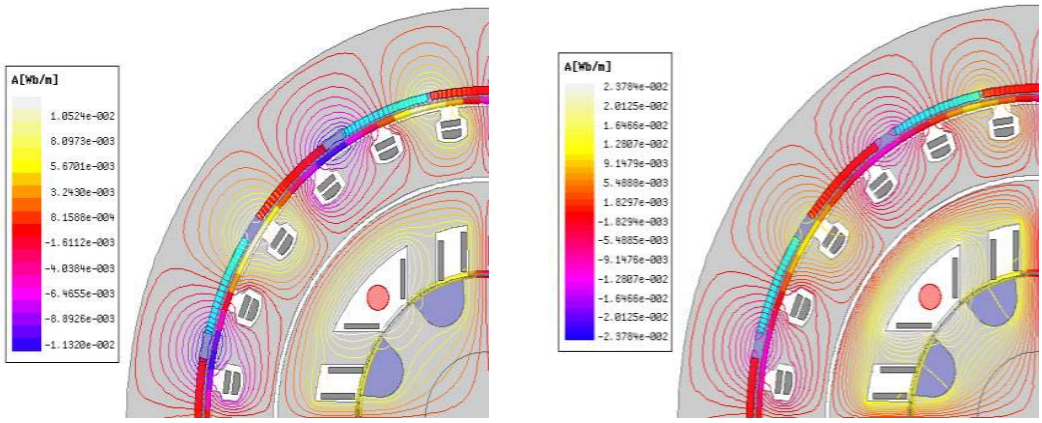

(a) (b)

Figure 11. Flux lines distribution with different excitation current. (a) $I_f = 5\,\mathrm{A}$. (b) $I_f = 10\,\mathrm{A}$.

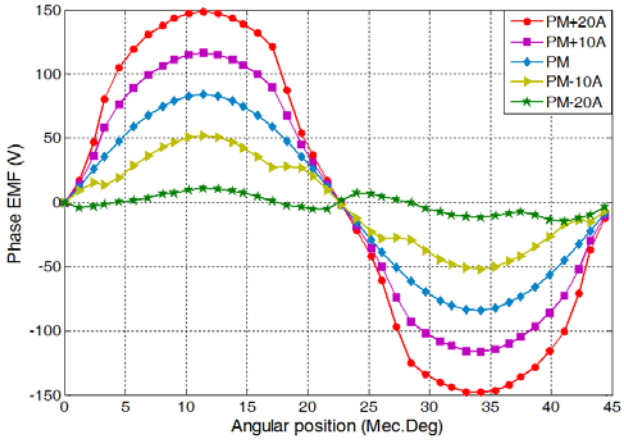

Figure 12. Phase-EMF waveforms.

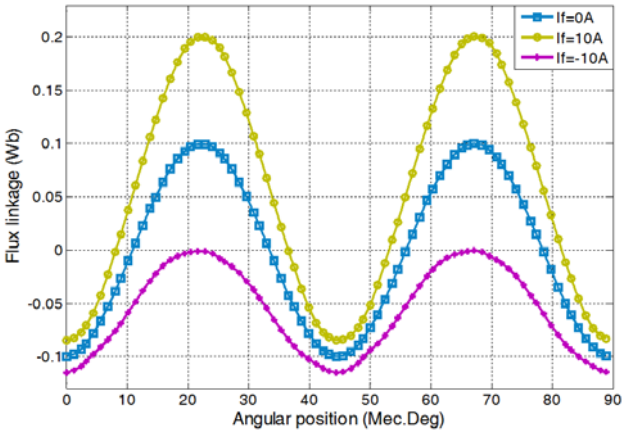

Figure 13. Flux linkage waveforms.

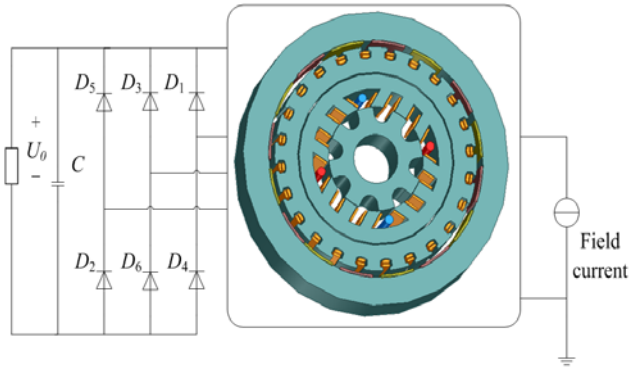

Figure 14. Field-circuit coupled model of DRHEM.

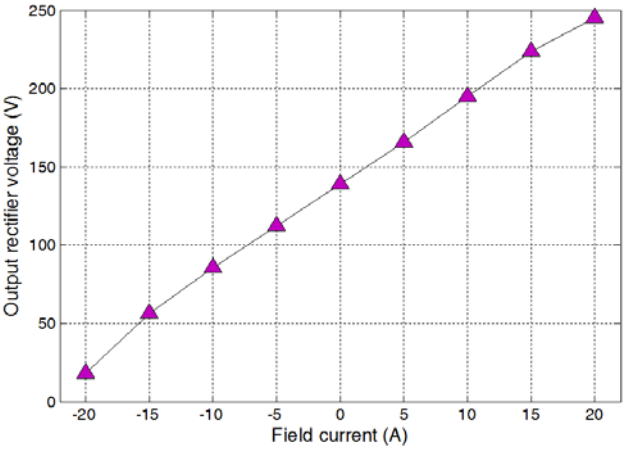

Figure 15. No-load characteristics of DRHEM.

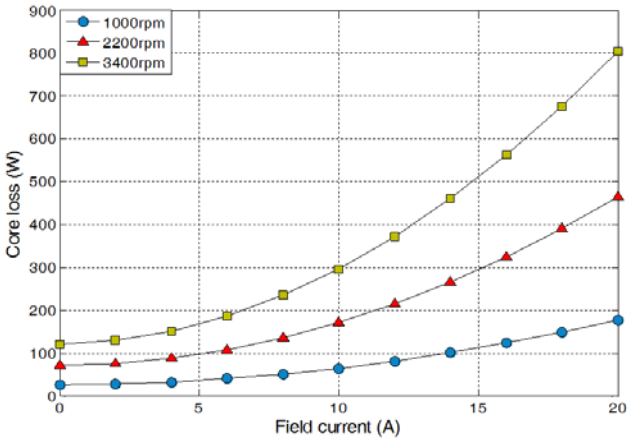

Figure 16. Core loss.

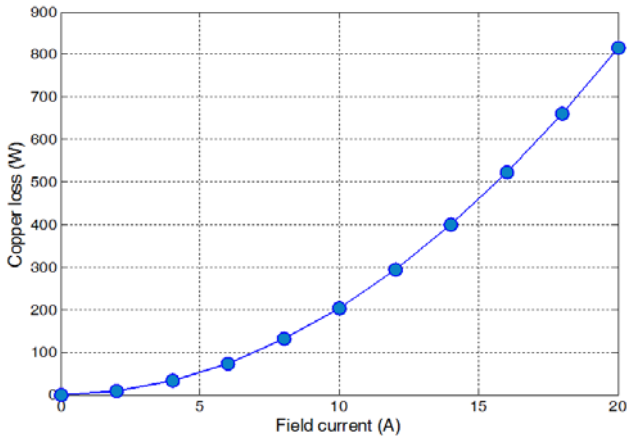

Figure 17. Copper loss.

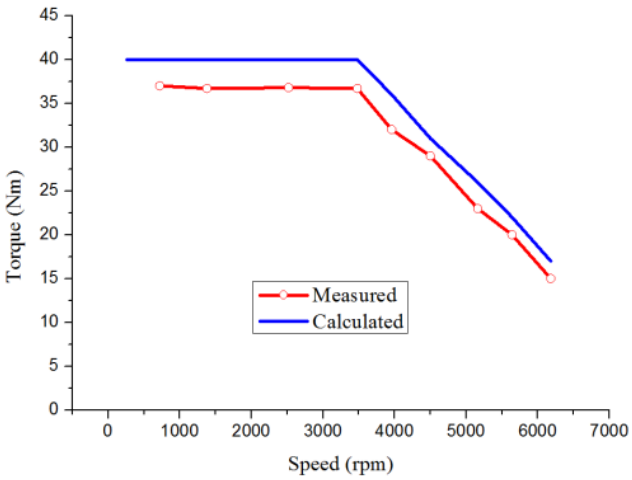

Figure 18. Torque-speed characteristics.

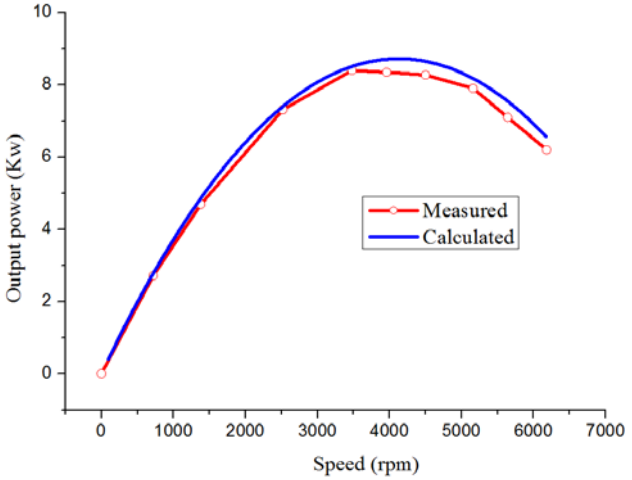

Figure 19. Output power-speed characteristics.

characteristics of DRHEM at 1000 rpm. The output rectifier voltage increases with the increase of excitation current, which is consistent with the principle of flux control.

Define voltage adjustment factor λ:

$$\lambda = \frac{U - U_0}{U_0} \tag{10}$$

where U is the DC output voltage, and U_0 is the DC output voltage at excitation current of 0. The voltage regulation factor changes from -59.5% to 76.9%, when the excitation current varies from -20 A to 20 A.

The motor loss directly affects the efficiency and temperature rise of the motor, which can be divided into mechanical loss and electromagnetic loss. Mechanical loss is mainly determined by the manufacturing process, and electromagnetic loss is mainly divided into copper loss and iron loss. Fig. 16 and Fig. 17 show the core loss and copper loss calculation results of the proposed motor at different excitation currents under no load operating, respectively. As a result of the excitation current increasing, both the core loss and copper loss will be boosted. In the case of $I_f = 0$ A, because of the existence of PM magnetic field, there is still a certain amount of iron loss, which is derived from the PM portion in the proposed motor. The change of motor speed will only affect the motor core loss but not the copper loss. The copper loss of the motor is determined by the winding resistance and current. So, the middle stator structure of the proposed DRHEM can shorten the end of the armature winding so as to achieve this effect of reducing the motor copper loss.

Then the analytically calculated and measured torque- and output power-speed characteristics are shown in Figs. 18–19. The analytically calculated and measured results agree well.

Figure 20 shows the efficiency of motor. It can be seen that the efficiency of motor is not affected by speed and that the motor has a smooth efficiency over a wide speed range.

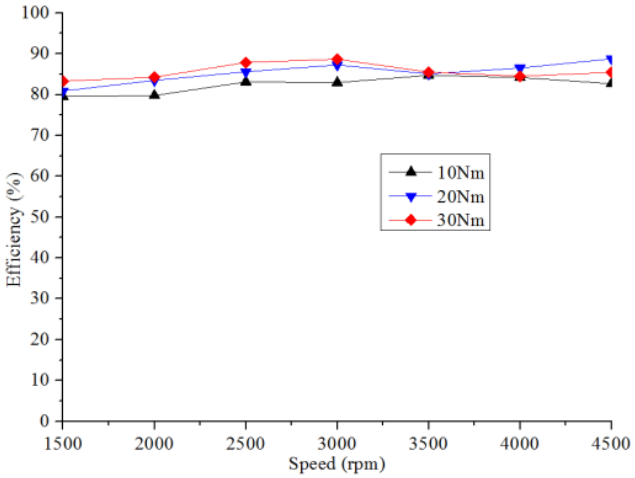

Figure 20. Efficiency.

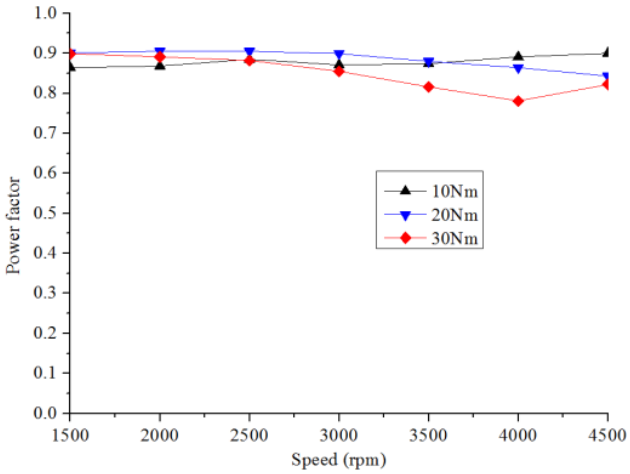

Figure 21. Power factor.

Figure 21 shows the curves of the power factor of the motor under different loads. As shown in Fig. 21, the maximum load power factor is up to 0.905. With the speed increasing, the power factor curve shows a slight downward trend.

5. CONCLUSION

This paper presents a new topology of the dual rotor hybrid excitation motor which combines PMSM and DSEM by a dual-rotor structure. In contrast to the previously published works for this topic, the proposed motor for flux density distribution analysis, MMF is presented as a whole, and the cogging torque of PMSM can be reduced by magnetic pole shift method. The phase EMF can be superimposed efficiently from the DSEM and PMSM portions. The result shows that the motor has a wide excitation regulation range. The proposed motor is further validated by experiments, and the performance results for various speeds are compared. The efficiency and power factor of the motor are without the effects of speed. Moreover, the theoretical analysis and experimental results indicate that the novel dual-rotor hybrid excitation brushless motor is suitable for aviation power supply starting system and electric vehicle.

ACKNOWLEDGMENT

This work was supported by the National Natural Science Foundation of China (Project No: 51707072), China Postdoctoral Science Foundation (Project No: 2018M632855), and the thesis Foundation of China Three Gorges University (Project no: 2018SSPY079).

REFERENCES

1. Xu, Z. G., S. J. Xie, and P. Mao, "Analytical design of flux-switching hybrid excitation machine by a nonlinear magnetic circuit method," *IEEE Trans. Magn.*, Vol. 49, No. 6, 3002–3008, Jun. 2013.
2. Zhang, Q., S. Huang, and G. D. Xie, "Design and experimental verification of hybrid excitation machine with isolated magnetic paths," *IEEE Trans. Energy Convers.*, Vol. 25, No. 4, 993–1000, Jun. 2010.

3. Chen, Z. H., Y. P. Sun, and Y. G. Yan, "Static characteristics of a novel hybrid excitation doubly salient machine," *International Conference on Electrical Machines and Systems. IEEE*, Jan. 2005.
4. Zhang, Z. R., J. Dai, and C. Dai, "Design considerations of a hybrid excitation synchronous machine with magnetic shunt rotor," *IEEE Trans. Magn.*, Vol. 49, No. 11, 5566–5573, May 2013.
5. Fodorean, D., A. Djerdir, and L. A. Viorel, "A double excited synchronous machine for direct drive application design and prototype tests," *IEEE Trans. Energy Convers.*, Vol. 22, No. 3, 656–665, Aug. 2007.
6. Owen, R. L., Z. Q. Zhu, and G. W. Jewell, "Hybrid-excited flux-switching permanent-magnet machines with iron flux bridges," *IEEE Trans. Magn.*, Vol. 46, No. 6, 1726–1729, May 2010.
7. Geng, W. W., Z. R. Zhang, and K. Jiang, "A new parallel hybrid excitation machine: permanent-magnet/variable-reluctance machine with bidirectional field-regulating capability," *IEEE Trans. Ind. Electro.*, Vol. 62, No. 3, 1372–1381, Aug. 2014.
8. Zhang, Z. R., Y. Y. Tao, and Y. G. Yan, "Investigation of a new topology of hybrid excitation doubly salient brushless DC generator," *IEEE Trans. Ind. Electro.*, Vol. 59, No. 6, 2550–2556, Jun. 2012.
9. Wang, Y. and Z. Deng, "Parallel hybrid excitation machines and their control schemes for DC generation system," *IET Electric Power Applications*, Vol. 6, No. 9, 669–680, Nov. 2012.
10. Afinowi, I. A. A., Z. Q. Zhu, and Y. Guan, "Hybrid-excited doubly salient synchronous machine with permanent magnets between adjacent salient stator poles," *IEEE Trans. Magn.*, Vol. 51, No. 10, ID: 8107909, Oct. 2015.
11. Cao, R. W., C. Mi, and M. Cheng, "Quantitative comparison of flux-switching permanent-magnet motors with interior permanent magnet motor for EV, HEV, and PHEV applications," *IEEE Trans. Magn.*, Vol. 48, No. 8, 2374–2383, Mar. 2012.
12. Zhu, S. S., C. Liu, and K. Wang, "Theoretical and experimental analyses of a hybrid excitation synchronous generator with integrated brushless excitation," *IET Electric Power Applications*, Vol. 10, No. 4, 258–267, Apr. 2016.
13. Fodorean, D., A. Djerdir, and L. A. Viorel, "A double excited synchronous machine for direct drive application — Design and prototype tests," *IEEE Trans. Energy Convers.*, Vol. 22, No. 3, 656–665, Aug. 2007.
14. Nedjar, B., S. Hlioui, and Y. Amara, "A new parallel double excitation synchronous machine," *IEEE Trans. Magn.*, Vol. 47, No. 9, 2252–2260, Apr. 2011.
15. Jing, L. B., T. Zhang, Y. Lin, and J. Cheng, "Design, analysis, and realization of a magnetic force transmission PM brushless motor," *IEEJ Trans. Electrical and Electronic Engineering*, Vol. 13, No. 5, 791–798, May 2018.
16. Wang, Q. S., S. X. Niu, and Y. Lin, "Design optimization and comparative study of novel dual-PM excited machines," *IEEE Trans. Ind. Electron.*, Vol. 64, No. 12, 9924–9933, Dec. 2017.
17. Sheng, T, T. and S. X. Niu, "Design of doubly complementary stator-PM machine with high magnet utilization factor for low-cost applications," *IEEE Trans. Energy Convers.*, Vol. 33, No. 2, 567–575, Jun. 2018.
18. Bianchi, N., M. Dai Pre, and Luigi, "Theory and design of fractional-slot PM machines," *CLEUP*, Padova, Italy, Sep. 2007.
19. Xu, Y., F. Wang, and K. Feng, "Analysis of inductance, permanent magnet EMF and slot torque ripple of dual-rotor permanent magnet machine," *Transactions of China Electro-technical Society*, Vol. 22, No. 9, 40–44, Sep. 2007.
20. Chen, Y., P. Pillay, and A. Khan, "PM wind generator comparison of different topologies," *39th IAS Annual Meeting, Conference Record of the 2004 IEEE*, Vol. 3, 1405–1412, 2004.
21. Zhang, F. G., J. H. Chen, and G. W. Liu, "Influence of stator fastener for permanent magnet machine with anti-rotation dual rotors," *Journal of Zhejiang University*, Vol. 45, No. 5, 804–808, May 2011.